

Correlated $\Lambda_c^+ \bar{\Lambda}_c^-$ production in e^+e^- annihilations at
 $\sqrt{s} \sim 10.5$ GeVCLEO Collaboration
(October 30, 2018)

Abstract

Using 13.6 fb^{-1} of continuum two-jet $e^+e^- \rightarrow c\bar{c}$ events collected with the CLEO detector, we have searched for baryon number correlations at the primary quark level. We have measured the likelihood for a Λ_c^+ charmed baryon to be produced in the hemisphere opposite a $\bar{\Lambda}_c^-$ relative to the likelihood for a Λ_c^+ charmed baryon to be produced opposite an anticharmed meson \bar{D} ; in all cases, the reconstructed hadrons must have momentum greater than $2.3 \text{ GeV}/c$. We find that, given a $\bar{\Lambda}_c^-$ (reconstructed in five different decay modes), a Λ_c^+ is observed in the opposite hemisphere $(0.72 \pm 0.11)\%$ of the time (not corrected for efficiency). By contrast, given a \bar{D} in one hemisphere, a Λ_c^+ is observed in the opposite hemisphere only $(0.21 \pm 0.02)\%$ of the time. Normalized to the total number of either $\bar{\Lambda}_c^-$ or \bar{D} “tags”, it is therefore $3.52 \pm 0.45 \pm 0.42$ times more likely to find a Λ_c^+ opposite a $\bar{\Lambda}_c^-$ than a \bar{D} meson. This enhancement is not observed in the JETSET 7.3 $e^+e^- \rightarrow c\bar{c}$ Monte Carlo simulation.

13.30.-a, 13.60.Rj, 13.65.+i, 14.20.Lq

A. Bornheim,¹ E. Lipeles,¹ S. P. Pappas,¹ M. Schmidtler,¹ A. Shapiro,¹ W. M. Sun,¹
 A. J. Weinstein,¹ D. E. Jaffe,² R. Mahapatra,² G. Masek,² H. P. Paar,² D. M. Asner,³
 A. Eppich,³ T. S. Hill,³ R. J. Morrison,³ R. A. Briere,⁴ G. P. Chen,⁴ T. Ferguson,⁴
 H. Vogel,⁴ A. Gritsan,⁵ J. P. Alexander,⁶ R. Baker,⁶ C. Bebek,⁶ B. E. Berger,⁶
 K. Berkelman,⁶ F. Blanc,⁶ V. Boisvert,⁶ D. G. Cassel,⁶ P. S. Drell,⁶ J. E. Duboscq,⁶
 K. M. Ecklund,⁶ R. Ehrlich,⁶ P. Gaidarev,⁶ R. S. Galik,⁶ L. Gibbons,⁶ B. Gittelman,⁶
 S. W. Gray,⁶ D. L. Hartill,⁶ B. K. Heltsley,⁶ P. I. Hopman,⁶ L. Hsu,⁶ C. D. Jones,⁶
 J. Kandaswamy,⁶ D. L. Kreinick,⁶ M. Lohner,⁶ A. Magerkurth,⁶ T. O. Meyer,⁶
 N. B. Mistry,⁶ E. Nordberg,⁶ M. Palmer,⁶ J. R. Patterson,⁶ D. Peterson,⁶ D. Riley,⁶
 A. Romano,⁶ J. G. Thayer,⁶ D. Urner,⁶ B. Valant-Spaight,⁶ G. Viehhauser,⁶
 A. Warburton,⁶ P. Avery,⁷ C. Prescott,⁷ A. I. Rubiera,⁷ H. Stoeck,⁷ J. Yelton,⁷
 G. Brandenburg,⁸ A. Ershov,⁸ D. Y.-J. Kim,⁸ R. Wilson,⁸ T. Bergfeld,⁹ B. I. Eisenstein,⁹
 J. Ernst,⁹ G. E. Gladding,⁹ G. D. Gollin,⁹ R. M. Hans,⁹ E. Johnson,⁹ I. Karliner,⁹
 M. A. Marsh,⁹ C. Plager,⁹ C. Sedlack,⁹ M. Selen,⁹ J. J. Thaler,⁹ J. Williams,⁹
 K. W. Edwards,¹⁰ R. Janicek,¹¹ P. M. Patel,¹¹ A. J. Sadoff,¹² R. Ammar,¹³ A. Bean,¹³
 D. Besson,¹³ P. Brabant,¹³ X. Zhao,¹³ S. Anderson,¹⁴ V. V. Frolov,¹⁴ Y. Kubota,¹⁴
 S. J. Lee,¹⁴ J. J. O'Neill,¹⁴ R. Poling,¹⁴ T. Riehle,¹⁴ A. Smith,¹⁴ C. J. Stepaniak,¹⁴
 J. Urheim,¹⁴ S. Ahmed,¹⁵ M. S. Alam,¹⁵ S. B. Athar,¹⁵ L. Jian,¹⁵ L. Ling,¹⁵ M. Saleem,¹⁵
 S. Timm,¹⁵ F. Wappler,¹⁵ A. Anastassov,¹⁶ E. Eckhart,¹⁶ K. K. Gan,¹⁶ C. Gwon,¹⁶
 T. Hart,¹⁶ K. Honscheid,¹⁶ D. Hufnagel,¹⁶ H. Kagan,¹⁶ R. Kass,¹⁶ T. K. Pedlar,¹⁶
 H. Schwarthoff,¹⁶ J. B. Thayer,¹⁶ E. von Toerne,¹⁶ M. M. Zoeller,¹⁶ S. J. Richichi,¹⁷
 H. Severini,¹⁷ P. Skubic,¹⁷ A. Undrus,¹⁷ V. Savinov,¹⁸ S. Chen,¹⁹ J. Fast,¹⁹ J. W. Hinson,¹⁹
 J. Lee,¹⁹ D. H. Miller,¹⁹ E. I. Shibata,¹⁹ I. P. J. Shipsey,¹⁹ V. Pavlunin,¹⁹
 D. Cronin-Hennessy,²⁰ A.L. Lyon,²⁰ E. H. Thorndike,²⁰ T. E. Coan,²¹ V. Fadeyev,²¹
 Y. S. Gao,²¹ Y. Maravin,²¹ I. Narsky,²¹ R. Stroynowski,²¹ J. Ye,²¹ T. Wlodek,²¹
 M. Artuso,²² C. Boulahouache,²² K. Bukin,²² E. Dambasuren,²² G. Majumder,²²
 G. C. Moneti,²² R. Mountain,²² S. Schuh,²² T. Skwarnicki,²² S. Stone,²² J.C. Wang,²²
 A. Wolf,²² J. Wu,²² S. Kopp,²³ M. Kostin,²³ A. H. Mahmood,²⁴ S. E. Csorna,²⁵ I. Danko,²⁵
 K. W. McLean,²⁵ Z. Xu,²⁵ R. Godang,²⁶ G. Bonvicini,²⁷ D. Cinabro,²⁷ M. Dubrovin,²⁷
 S. McGee,²⁷ and G. J. Zhou²⁷

¹California Institute of Technology, Pasadena, California 91125

²University of California, San Diego, La Jolla, California 92093

³University of California, Santa Barbara, California 93106

⁴Carnegie Mellon University, Pittsburgh, Pennsylvania 15213

⁵University of Colorado, Boulder, Colorado 80309-0390

⁶Cornell University, Ithaca, New York 14853

⁷University of Florida, Gainesville, Florida 32611

⁸Harvard University, Cambridge, Massachusetts 02138

⁹University of Illinois, Urbana-Champaign, Illinois 61801

¹⁰Carleton University, Ottawa, Ontario, Canada K1S 5B6
and the Institute of Particle Physics, Canada

¹¹McGill University, Montréal, Québec, Canada H3A 2T8
and the Institute of Particle Physics, Canada

¹²Ithaca College, Ithaca, New York 14850

¹³University of Kansas, Lawrence, Kansas 66045

¹⁴University of Minnesota, Minneapolis, Minnesota 55455

- ¹⁵State University of New York at Albany, Albany, New York 12222
¹⁶Ohio State University, Columbus, Ohio 43210
¹⁷University of Oklahoma, Norman, Oklahoma 73019
¹⁸University of Pittsburgh, Pittsburgh, Pennsylvania 15260
¹⁹Purdue University, West Lafayette, Indiana 47907
²⁰University of Rochester, Rochester, New York 14627
²¹Southern Methodist University, Dallas, Texas 75275
²²Syracuse University, Syracuse, New York 13244
²³University of Texas, Austin, Texas 78712
²⁴University of Texas - Pan American, Edinburg, Texas 78539
²⁵Vanderbilt University, Nashville, Tennessee 37235
²⁶Virginia Polytechnic Institute and State University, Blacksburg, Virginia 24061
²⁷Wayne State University, Detroit, Michigan 48202

I. INTRODUCTION

At high energy, quark fragmentation can be calculated using Perturbative QCD (PQCD). The results are often referred to as QCD showers [1]. However, these calculations require, for comparison with experimental results, some model or experimental input to take into account the eventual hadronization of gluons and $q\bar{q}$ pairs into actual hadrons of known mass.

Several models have thus been developed, mostly based on a chromodynamic string connecting the initial q_0 and \bar{q}_0 [2–6], where the subscript indicates that these are the primary quarks formed by e^+e^- annihilation. When stretched because of the initial momentum of q_0 and \bar{q}_0 , the string breaks by creation of secondary $q\bar{q}$ pairs, generating two substrings. The process iterates then for the new substrings until the physical hadrons are produced. This last stage is the critical one where QCD loses its predictive power.

The model most frequently used to simulate the process $e^+e^- \rightarrow q_0\bar{q}_0 \rightarrow \text{hadrons}$ is the QCD inspired Lund String Model (LSM) [2], implemented in the Jetset Monte Carlo simulation package [7]. In order to solve the problem of generating hadrons of known mass, the Jetset implementation of LSM, at each step of its iterative process, splits a $q\bar{q}$ string into a hadron of known quantum numbers and mass and a remainder string having the leftover quantum numbers and energy-momentum. When, finally, the remainder string has a mass below a suitable limit, this string is made into two known hadrons that, together, carry the leftover quantum numbers.

In this paper we report on correlations between charm baryons in the fragmentation of a $c\bar{c}$ system produced in the reaction $e^+e^- \rightarrow c\bar{c}$ at $\sqrt{s} \sim 10$ GeV, where the annihilation occurs in a largely low- Q^2 , non-perturbative regime. In contrast to inclusive single-particle production, compensation of baryon and charm number is a more subtle aspect of quark fragmentation modeling. One obvious question is whether baryon compensation occurs locally (e.g., small rapidity difference between baryon and antibaryon) or globally (large rapidity difference). Previous studies of $\Lambda\bar{\Lambda}$ production at $\sqrt{s}=90$ GeV found that in events containing both a Λ and a $\bar{\Lambda}$, the two particles tended to be produced at very similar rapidities [8].

Consider the case in which a charm baryon is produced in the first step of fragmentation (e.g. $e^+e^- \rightarrow c\bar{c}$; $c \rightarrow \Lambda_c X$); it is possible that both baryon and quantum charm numbers be compensated in the opposite hemisphere (e.g. $e^+e^- \rightarrow c\bar{c}$; $c \rightarrow \Lambda_c X$, $\bar{c} \rightarrow \bar{\Lambda}_c^- X$). In the limit that the c and \bar{c} quarks fragment independently (presumably true at some sufficiently high energy), this

type of correlation is not expected. The Jetset implementation of the Lund model, because of the mechanism outlined above, does not produce such a correlation.

In the very reasonable approximation of neglecting string splitting by $c\bar{c}$ tunneling from the vacuum, at $\sqrt{s} \sim 10$ GeV all observed charmed particles must contain a primary quark. We take advantage of this to discriminate between independent vs. correlated fragmentation models. If we assume that primary quarks fragment independently, then the number of times that we find a Λ_c^+ baryon opposite a $\bar{\Lambda}_c^-$ antibaryon in an event (i.e., $\cos\theta(\Lambda_c^+, \bar{\Lambda}_c^-) < 0$, denoted “ $\Lambda_c^+|\bar{\Lambda}_c^-$ ”), scaled to the total number of observed $\bar{\Lambda}_c^-$ (denoted “ $\frac{\Lambda_c^+|\bar{\Lambda}_c^-}{\bar{\Lambda}_c^-}$ ”), should be equal to the number of times that we find a Λ_c^+ baryon opposite any other anti-charmed hadron \bar{H}_c , scaled to the total number of observed anti-charmed hadrons ($\frac{\Lambda_c^+|\bar{H}_c}{\bar{H}_c}$). In this analysis, we will check the equality of these ratios; by comparing ratios in this way, we cancel many experimental systematics. Schematically, we are comparing the following event topologies:

$$\bar{\Lambda}_c^- \leftrightarrow \begin{array}{c} \bar{c} \ c \\ \hline \end{array} \leftrightarrow \Lambda_c^+$$

vs

$$\bar{H}_c \leftrightarrow \begin{array}{c} \bar{c} \ c \\ \hline \end{array} \leftrightarrow \Lambda_c^+$$

Specifically, we compare the rate of $\Lambda_c^+|\bar{\Lambda}_c^-$ production to the rate of $\Lambda_c^+|\bar{D}^0$ and $\Lambda_c^+|D^-$ production. We reconstruct \bar{D}^0 's and D^- 's through the well-measured decay modes $\bar{D}^0 \rightarrow K^+\pi^-$ and $D^- \rightarrow K^+\pi^-\pi^-$, respectively. Λ_c^+ 's are fully reconstructed in the decay modes $\Lambda_c^+ \rightarrow pK^-\pi^+$, $\Lambda_c^+ \rightarrow pK_s^0$, $\Lambda_c^+ \rightarrow \Lambda\pi^+$, $\Lambda_c^+ \rightarrow \Lambda\pi^+\pi^-\pi^+$, $\Lambda_c^+ \rightarrow pK_s^0\pi^+\pi^-$,¹ and partially reconstructed through $\Lambda_c^+ \rightarrow \Lambda X$.² Σ_c 's are also studied; these are reconstructed in $\Sigma_c^{++} \rightarrow \Lambda_c^+\pi^+$ and $\Sigma_c^0 \rightarrow \Lambda_c^+\pi^-$.

Under the assumption of independent fragmentation, we expect the relative production ratios to satisfy:

$$\frac{\Lambda_c^+|\bar{\Lambda}_c^-}{\bar{\Lambda}_c^-} \div \frac{\Lambda_c^+|\bar{D}^0}{\bar{D}^0} = 1$$

and,

$$\frac{\Lambda_c^+|\bar{\Lambda}_c^-}{\bar{\Lambda}_c^-} \div \frac{\Lambda_c^+|D^-}{D^-} = 1.$$

¹Charge conjugation is implicit.

²According to JETSET 7.3 simulations, 95% of the Λ 's opposite an anti-charm tag are charmed baryon daughters (predominantly Λ_c) after imposing a 1 GeV/c minimum momentum requirement on the Λ ($p_\Lambda > 1$ GeV/c).

II. APPARATUS AND EVENT SELECTION

This analysis was performed using the CLEO II and the upgraded CLEO II.V detectors operating at the Cornell Electron Storage Ring (CESR) at center-of-mass energies $\sqrt{s} = 10.52\text{--}10.58$ GeV. For 4.5 fb^{-1} of the data used for this analysis (“CLEO-II” data [9]), measurements of charged particle momenta were made with three nested coaxial drift chambers consisting of 6, 10, and 51 layers, respectively. In a subsequent upgrade (“CLEO-II.V” [10]), the inner tracking chamber was replaced with a high-precision silicon detector (corresponding to the remaining 9.1 fb^{-1} of the data used for this analysis). The entire tracking system fills the volume from $r=3$ cm to $r=1$ m, with r the radial coordinate relative to the beam (\hat{z}) axis. This system is very efficient ($\epsilon \geq 98\%$) for detecting tracks that have transverse momenta (p_T) relative to the beam axis greater than 200 MeV/c, and that are contained within the good fiducial volume of the drift chamber ($|\cos\theta| < 0.94$, with θ defined as the polar angle relative to the beam axis). This system achieves a momentum resolution of $(\delta p/p)^2 = (0.0015p)^2 + (0.005)^2$ (p is the momentum, measured in GeV/c). Pulse-height measurements in the main drift chamber provide specific ionization resolution of 5.0% (CLEO II.V) or 5.5% (CLEO II) for Bhabha events, giving good K/π separation for tracks with momenta up to 700 MeV/c and separation of order 2σ in the relativistic rise region above 2.5 GeV/c. Outside the central tracking chambers are plastic scintillation counters, which are used as a fast element in the trigger system and also provide particle identification information from time-of-flight measurements.

Beyond the time-of-flight system is the electromagnetic calorimeter, consisting of 7800 thallium-doped CsI crystals. The central “barrel” region of the calorimeter covers about 75% of the solid angle and has an energy resolution which is empirically found to follow:

$$\frac{\sigma_E}{E}(\%) = \frac{0.35}{E^{0.75}} + 1.9 - 0.1E; \quad (1)$$

E is the shower energy in GeV. This parameterization includes noise effects, and translates to an energy resolution of about 4% at 100 MeV and 1.2% at 5 GeV. Two end-cap regions of the crystal calorimeter extend solid angle coverage to about 95% of 4π , although energy resolution is not as good as that of the barrel region. The tracking system, time-of-flight counters, and calorimeter are all contained within a superconducting coil operated at 1.5 Tesla. An iron flux return interspersed with proportional tubes used for muon detection is located immediately outside the coil and in the two end-cap regions.

The event sample used for this measurement is comprised of 9.1 fb^{-1} of data collected at the $\Upsilon(4S)$ resonance and 4.5 fb^{-1} of data collected about 60 MeV below the $\Upsilon(4S)$ resonance. Approximately 18×10^6 continuum $c\bar{c}$ events are included in this sample. Charged track candidates for protons, kaons or pions must pass the following restrictions:

(a) The track must have an impact parameter relative to the estimated event vertex less than 5 mm in a plane perpendicular to the beam axis ($\hat{r} - \hat{\phi}$) and no more than 5 cm along the beam axis. The estimated event vertex is obtained by averaging the e^+e^- interaction point over a full run.

(b) The track has specific ionization information consistent (at the 99% confidence level) with its assumed particle identity.

(c) The track must have momentum greater than 100 MeV/c.

All reconstructed charmed hadrons must have momentum greater than 2.3 GeV/c to ensure that there is no contamination from B -meson decays to charm.

A. Production Ratios

We define the single tag yield to be the number of reconstructed events containing one anti-charmed hadron \overline{H}_c . This yield (Table I) is determined by fitting a double-Gaussian signal over a smooth, low-order polynomial background functional. The signal function is the sum of two Gaussian functions, one narrow and one broad, and is a better representation of the expected signal line shape than a single Gaussian function.

TABLE I. Single Tag Yields obtained from one-dimensional fits (charge conjugate modes are implied); statistical errors only are shown.

	Data	Monte Carlo
	(~ 60 M hadronic events)	(~ 160 M hadronic events)
Λ_c (5 modes)	70199 ± 1604	
Λ_c ($pK^-\pi^+ + pK_s^0$ only)	56110 ± 1776	130380 ± 1943
$\Sigma_c^0 \rightarrow \Lambda_c^+\pi^- + \Sigma_c^{++} \rightarrow \Lambda_c^+\pi^+$ (sum)	3804 ± 185	6522 ± 182
$\Lambda \rightarrow p\pi^-$	735343 ± 1198	2136997 ± 1674
$D^0 \rightarrow K^-\pi^+$	352294 ± 1668	1045776 ± 2294
$D^+ \rightarrow K^-\pi^+\pi^+$	273597 ± 2148	705357 ± 3232

The number of double tags (Table II) is defined as the number of events in which two specific particles are reconstructed in opposite hemispheres (i.e., the opening angle between the two particles must be greater than 90 degrees). The total number of double tags for $\Lambda_c^+|\overline{\Lambda}_c^-$, $\Lambda_c^+|\overline{\Lambda}$, $\Lambda_c^+|\overline{D}^0$ and $\Lambda|\overline{D}^0$ is extracted from two-dimensional invariant mass plots, shown in Figures 1, 2, 3, and 4 respectively.

The total correlated double-tag yield is first determined by performing a sideband subtraction in the two-dimensional invariant mass plot. Consider, for example Fig. 1. We take one-dimensional projections of three slices in the candidate $\overline{\Lambda}_c^-$ recoil invariant mass “ M_{recoil} ” - the $\overline{\Lambda}_c^-$ signal region: ($|M_{recoil} - 2.286| < 0.03 \text{ GeV}/c^2$) and the two $\overline{\Lambda}_c^-$ sideband regions: ($0.04 < |M_{recoil} - 2.286| < 0.07 \text{ GeV}/c^2$). We then subtract the Λ_c^+ distributions from the $\overline{\Lambda}_c^-$ sidebands from that of the $\overline{\Lambda}_c^-$ signal region. Figure 5. shows the signal distribution and the sum of the two sideband distributions. In performing these fits, the double-Gaussian signal shapes are constrained using the parameters determined from fits to the single-tag sample.

We also perform a single fit in two dimensions to extract the signal yields. In this latter fit, a two-dimensional Gaussian signal is used to parametrize the peak region, two single Gaussians are used to fit the “ridges” away from the peak region (corresponding to true charmed hadrons along one axis in association with combinatoric background on the other axis) and a two-dimensional, smooth polynomial is used to parametrize the background. Differences in i) the selection of the sideband/signal regions and the regions projected, as well as ii) the difference between the sideband-subtracted yield compared to the two-dimensional, single-fit yield give a measure of the fitting systematics for each measurement.

We define the “production rate” (Table III) as the percentage of times we find one specific particle in an event opposite a given tag (i.e., the number of double tags, given in Table II divided by the total number of single tags, presented in Table I). Production ratios are formed by taking

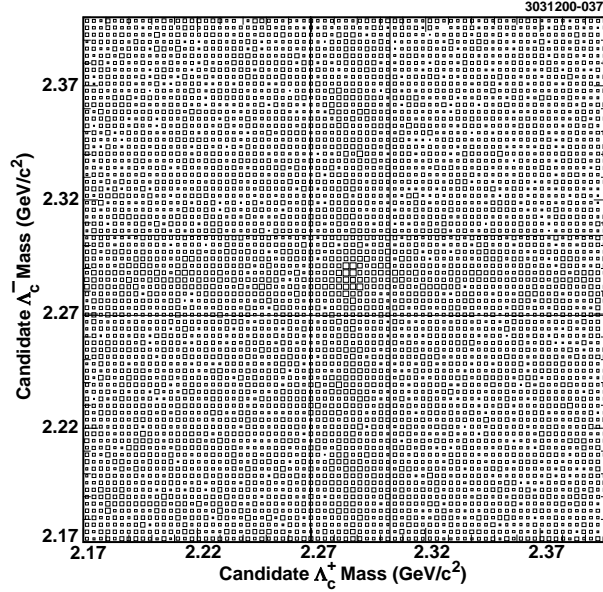


FIG. 1. Double tag invariant mass plot of Λ_c^+ candidates plotted vs. invariance mass of Λ_c^- candidates ($\Lambda_c^+|\Lambda_c^-$) from data. Shown is the sum of the modes: $\Lambda_c^+ \rightarrow pK^-\pi^+$, $\Lambda_c^+ \rightarrow pK_s^0$, $\Lambda_c^+ \rightarrow \Lambda\pi^+$, $\Lambda_c^+ \rightarrow \Lambda\pi^+\pi^-\pi^+$, and $\Lambda_c^+ \rightarrow pK_s^0\pi^+\pi^-$ (and their charge conjugates, in the case of Λ_c^- reconstruction). Horizontal and vertical solid lines designate signal bands.

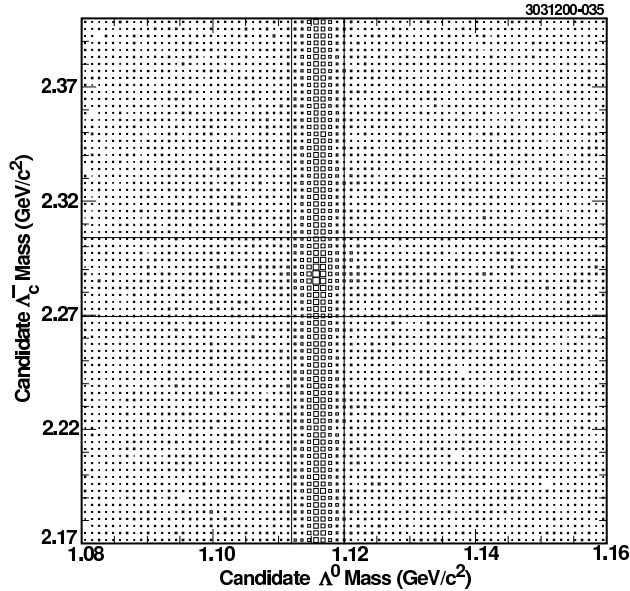


FIG. 2. Double tag plot of $\Lambda|\Lambda_c^-$ (plus charge conjugate) from data. The Λ_c^- is selected as in the previous figure; the Λ is reconstructed in $\Lambda \rightarrow p\pi$. Horizontal and vertical solid lines designate signal bands.

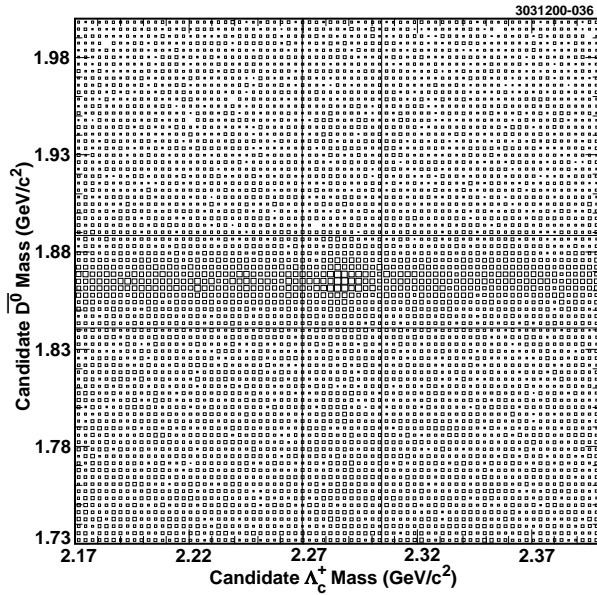


FIG. 3. Double tag plot of $\Lambda_c^+ |D^0$ (plus charge conjugate) for data. Horizontal and vertical solid lines designate signal bands.

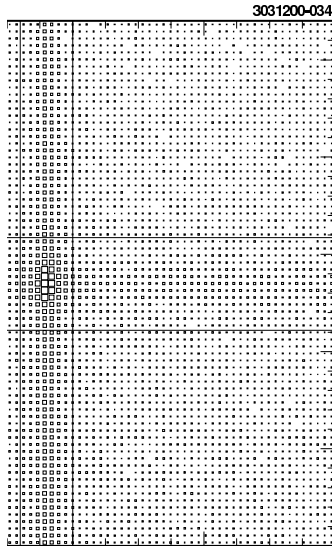


FIG. 4. Double tag plot of $\Lambda |D^0$ (plus charge conjugate) for data. Horizontal and vertical solid lines designate signal bands.

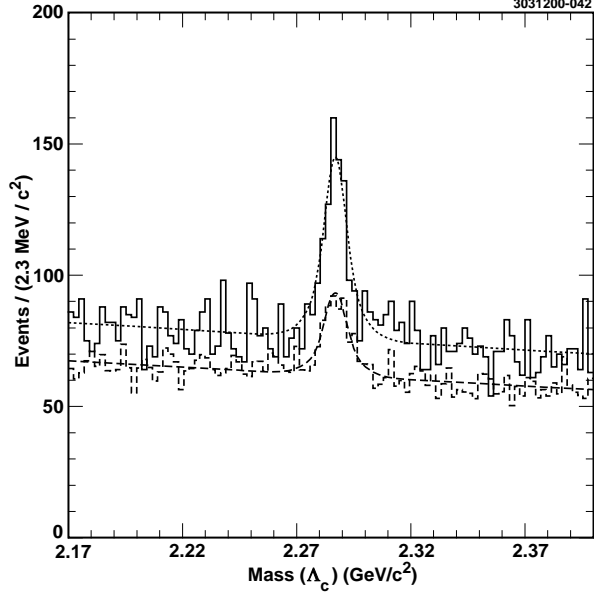


FIG. 5. Projections of Figure 1 onto the candidate Λ_c^+ mass, after requiring that the recoil mass be consistent with the $\overline{\Lambda}_c^-$ signal (solid histogram, with dotted curve fit overlaid) and sideband (dashed) regions (see text for details).

TABLE II. Double Tag Yields obtained from two-dimensional fits (statistical errors only).

	Data	Monte Carlo
$\Lambda_c^+ \overline{\Lambda}_c^-$	253 ± 37	97 ± 40
$\Lambda_c^+ \overline{D}^0$	722 ± 55	1905 ± 78
$\Lambda_c^+ D^-$	556 ± 71	1281 ± 96
$\Lambda_c^+ \overline{\Sigma}_c$	34 ± 14	13 ± 9
$\Lambda_c^+ \overline{\Lambda}$	1355 ± 72	1079 ± 85
$\Sigma_c \overline{D}^0$	29 ± 13	88 ± 13
$\Sigma_c D^-$	32 ± 18	59 ± 14
$\Sigma_c \overline{\Lambda}$	122 ± 19	49 ± 12
$\Lambda \overline{D}^0$	2400 ± 69	8547 ± 117
ΛD^-	2132 ± 90	6397 ± 144

ratios of production rates (Table IV). Note that, to compare $\frac{\Lambda_c^+|\bar{\Lambda}_c^-}{\bar{\Lambda}_c^-}$ to $\frac{\Lambda_c^+|\bar{D}}{\bar{D}}$, we must take into account the fact that the latter ratio implicitly includes both sign combinations ($\frac{\Lambda_c^+|\bar{D}}{\bar{D}}$ plus $\frac{\bar{\Lambda}_c^-|D}{D}$), while there is only one unique way to form $\frac{\Lambda_c^+|\bar{\Lambda}_c^-}{\bar{\Lambda}_c^-}$. To compare these two rates and form production ratios (Table IV), the production rates for $\bar{\Lambda}_c^-$ -tags presented in the table have therefore been multiplied by this factor of two.

TABLE III. Production Rates; statistical errors only.

$\frac{\text{Double tags}}{\text{Single tags}}$	Data Fraction	Monte Carlo Fraction
$2 \times \frac{\Lambda_c^+ \bar{\Lambda}_c^-}{\bar{\Lambda}_c^-}$	$(7.19 \pm 1.08) \times 10^{-3}$	$(1.49 \pm 0.62) \times 10^{-3}$
$\frac{\Lambda_c^+ D^0}{D^0}$	$(2.05 \pm 0.16) \times 10^{-3}$	$(1.82 \pm 0.08) \times 10^{-3}$
$\frac{\Lambda_c^+ D^-}{D^-}$	$(2.03 \pm 0.26) \times 10^{-3}$	$(1.82 \pm 0.14) \times 10^{-3}$
$\frac{\Lambda \bar{\Lambda}_c^-}{\bar{\Lambda}_c^-}$	$(19.3 \pm 1.1) \times 10^{-3}$	$(8.28 \pm 0.66) \times 10^{-3}$
$\frac{\Sigma_c \bar{\Lambda}_c^-}{\bar{\Lambda}_c^-}$	$(0.49 \pm 0.20) \times 10^{-3}$	$(0.102 \pm 0.066) \times 10^{-3}$
$\frac{\Sigma_c D^0}{D^0}$	$(0.082 \pm 0.036) \times 10^{-3}$	$(0.068 \pm 0.008) \times 10^{-3}$
$\frac{\Sigma_c D^-}{D^-}$	$(0.067 \pm 0.049) \times 10^{-3}$	$(0.084 \pm 0.020) \times 10^{-3}$
$\frac{\Lambda \bar{\Sigma}_c}{\bar{\Sigma}_c}$	$(32.1 \pm 5.2) \times 10^{-3}$	$(7.6 \pm 1.8) \times 10^{-3}$
$\frac{\Lambda D^0}{D^0}$	$(6.81 \pm 0.20) \times 10^{-3}$	$(8.17 \pm 0.11) \times 10^{-3}$
$\frac{\Lambda D^-}{D^-}$	$(7.79 \pm 0.33) \times 10^{-3}$	$(9.07 \pm 0.21) \times 10^{-3}$

TABLE IV. Production Ratios

	Data (stat. and sys. errors)	Monte Carlo (stat. error only)
$\frac{2 \times \Lambda_c^+ \bar{\Lambda}_c^-}{\bar{\Lambda}_c^-} \div \frac{\Lambda_c^+ D^0}{D^0}$	$(3.51 \pm 0.59 \pm 0.42)$	(0.82 ± 0.34)
$\frac{2 \times \Lambda_c^+ \bar{\Lambda}_c^-}{\bar{\Lambda}_c^-} \div \frac{\Lambda_c^+ D^-}{D^-}$	$(3.54 \pm 0.70 \pm 0.43)$	(0.80 ± 0.35)
$\frac{\Lambda \bar{\Lambda}_c^-}{\bar{\Lambda}_c^-} \div \frac{\Lambda D^0}{D^0}$	$(2.83 \pm 0.18 \pm 0.26)$	(1.01 ± 0.08)
$\frac{\Lambda \bar{\Lambda}_c^-}{\bar{\Lambda}_c^-} \div \frac{\Lambda D^-}{D^-}$	$(2.48 \pm 0.18 \pm 0.23)$	(0.91 ± 0.08)
$\frac{\Lambda \bar{\Sigma}_c}{\bar{\Sigma}_c} \div \frac{\Lambda D^0}{D^0}$	$(4.71 \pm 0.77 \pm 0.56)$	(0.93 ± 0.22)
$\frac{\Lambda \bar{\Sigma}_c}{\bar{\Sigma}_c} \div \frac{\Lambda D^-}{D^-}$	$(4.12 \pm 0.68 \pm 0.52)$	(0.84 ± 0.22)

From Table III, we see a clear enhancement in the likelihood of producing a Λ_c^+ opposite a $\bar{\Lambda}_c^-$ compared to a \bar{D} . This is observed in the case where the Λ_c^+ is fully reconstructed, as well as tagged inclusively by a Λ . Note that the fractional enhancement is smaller in the case when the Λ_c^+ is tagged inclusively. This is qualitatively consistent with the expectation that events containing two

charmed mesons and two baryons will produce a $\Lambda|\overline{D}$ correlation which will inflate the denominator when we construct the ratio: $\frac{\Lambda|\overline{\Lambda}_c^-}{\overline{\Lambda}_c^-} / \frac{\Lambda|\overline{D}}{D}$. Non-cancelling contributions to the numerator, such as $\Lambda K\overline{N}D|\overline{\Lambda}_c^-$, plus decays of charmed baryons other than Λ_c into Λ , may also be present.

III. CROSS CHECKS

A number of cross checks were conducted in order to verify the accuracy of the double tag signal extraction. These include signal extractions of two-dimensional “wrong sign” plots (expected to have zero signal yield), as well as consistency checks with Monte Carlo and studies of $D|\overline{D}$ correlations.

A. Null and Wrong sign signals

Neglecting the doubly Cabibbo suppressed decay $\overline{D}^0 \rightarrow K^-\pi^+$, we expect a null signal yield from a double tag plot of $(m_{K^-\pi^+}|m_{K^-\pi^+})$. Similarly, we expect zero signal yield from a double tag plot of $(m_{K^-\pi^+}m_{K^+\pi^-}|)$ in the case where the D^0 and \overline{D}^0 candidate are in the same hemisphere. All of these correlations give signal yields consistent with zero as expected (Table V).

TABLE V. Null Checks (statistical errors only).

Correlation	Yield
$D^0 D^0$ (opposite hemisphere)	-16 ± 47
$D^\pm D^\pm$ (opposite hemisphere)	-10 ± 83
$D^0 D^+$ (opposite hemisphere)	55 ± 91
$D^0\overline{D}^0 $ (same hemisphere)	-15 ± 25
$D^\pm D^\mp $ (same hemisphere)	-116 ± 157

B. Monte Carlo studies

The uncertainty in Λ_c production characteristics is expected to be somewhat larger than the uncertainty in D^0 production. We therefore expect the Monte Carlo and data to agree on, e.g., the number of $D^+|D^-$ double tags per D^- ($\frac{D^+|D^-}{D^-}$), and the number of $D^0|\overline{D}^0$ double tags (Figure 6) per \overline{D}^0 ($\frac{D^0|\overline{D}^0}{\overline{D}^0}$), as shown in Table VI.³

Within errors, the agreement is good. We have also further ensured that there is no bias in the signal extraction due to possible peaking of the background in the signal region, by subtracting all the true signal from a Monte Carlo double tag plot and verifying that the measured yield, after subtraction of the true generated particles, is indeed consistent with zero.

³The measured value of 0.0119, for instance, is qualitatively consistent with the expectation that, per \overline{D}^0 tag, 50% of the time the charm quark will produce a D^0 , which is reconstructed in the $D^0 \rightarrow K^-\pi^+$ mode ($\mathcal{B}(D^0 \rightarrow K^-\pi^+) \sim 0.04$) with approximately 60% efficiency.

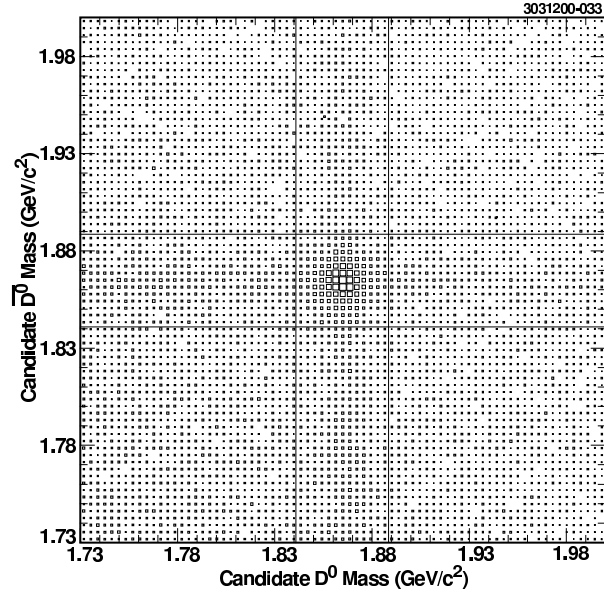


FIG. 6. Double tag plot of $D^0|\overline{D}^0$. Horizontal and vertical solid lines designate signal bands.

TABLE VI. Consistency Check using $D|\overline{D}$ correlations (statistical errors only).

	Data Raw Rate	Monte Carlo Raw Rate
$D^0 \overline{D}^0$ yield	2099 ± 56	6238 ± 97
$\frac{D^0 \overline{D}^0}{D^0}$ production rate	0.0119 ± 0.0003	0.0119 ± 0.0002
$D^+ D^-$ yield	1260 ± 88	3279 ± 130
$\frac{D^+ D^-}{D^-}$ production rate	0.0092 ± 0.0006	0.0093 ± 0.0004

C. Check of expected uncorrelated yield

Having obtained values for production rates, we can compare these with the values expected under the assumption of two hemispheres fragmentating independently. In this (hypothetical) limit, the ratio of double-tags to single-tags should be the same as the ratio of single-tags to total charm quarks, since each simply expresses the probability of a charm quark to evolve into a particular final-state particle. Then, using $\mathcal{B}(\Lambda_c \rightarrow X)$ to designate the branching fraction for Λ_c to decay into the final state X , \mathcal{L} as the integrated luminosity of our data set, and $f_{(c \rightarrow \Lambda_c)}$ as the fraction of times a charm quark materializes as a Λ_c baryon, we can relate the expected number of single tags and double tags as:

$$N(\Lambda_c)_{Single\ Tags} = \mathcal{L} \cdot \sigma(e^+e^- \rightarrow c\bar{c}) \cdot f_{(c \rightarrow \Lambda_c)} \cdot \mathcal{B}(\Lambda_c \rightarrow X) \cdot \epsilon_{\Lambda_c \rightarrow X} \quad (2)$$

and, for the probability that, given a reconstructed Λ_c , we reconstruct an opposite $\bar{\Lambda}_c^-$

$$N(\Lambda_c^+|\bar{\Lambda}_c^-)_{Double\ Tags} = f'_{(c \rightarrow \Lambda_c)} \cdot \mathcal{B}(\Lambda_c \rightarrow X) \cdot \epsilon'_{\Lambda_c \rightarrow X} \cdot N(\Lambda_c)_{Single\ Tags} \quad (3)$$

In equation (2), for the number of single Λ_c^+ tags, we use half the total number of observed $\Lambda_c^+ + \bar{\Lambda}_c^-$ (70199/2). In equation (3), the term $f'_{(c \rightarrow \Lambda_c)}$ indicates that the fraction of times that a charm quark produces a Λ_c may be different if the event already contains a $\bar{\Lambda}_c$ produced from the corresponding anticharm quark. This is, of course, exactly the correlation factor we wish to ultimately measure. The prime on $\epsilon'_{\Lambda_c \rightarrow X}$ indicates that the efficiency for reconstructing a Λ_c may be higher for events in which a $\bar{\Lambda}_c$ has already been reconstructed due to geometrical correlations – since the charm and anticharm quarks are back to back in an $e^+e^- \rightarrow c\bar{c}$ event, reconstruction of one charmed particle ensures that the corresponding antiparticle is in a good acceptance region of the detector. Dividing equation (3) by equation (2) and multiplying each side by $N(\Lambda_c)_{Single\ Tags}$ we obtain, for the number of double tags:

$$N(\Lambda_c^+|\bar{\Lambda}_c^-)_{DoubleTags} = \frac{(N(\Lambda_c)_{SingleTags})^2 \cdot f'_{(c \rightarrow \Lambda_c)} \cdot \epsilon'_{\Lambda_c \rightarrow X}}{\mathcal{L} \cdot \sigma(e^+e^- \rightarrow c\bar{c}) \cdot f_{(c \rightarrow \Lambda_c)} \cdot \epsilon_{\Lambda_c \rightarrow X}} \quad (4)$$

The difference between $f_{(c \rightarrow \Lambda_c)}$ and $f'_{(c \rightarrow \Lambda_c)}$ represents the enhancement in production of the Λ_c when a $\bar{\Lambda}_c$ is present. With $\frac{\epsilon'_{\Lambda_c \rightarrow X}}{\epsilon_{\Lambda_c \rightarrow X}} \equiv \epsilon_{geometry}$ and $\frac{f'_{(c \rightarrow \Lambda_c)}}{f_{(c \rightarrow \Lambda_c)}} \equiv f_{correlated}$ (=1 if independent fragmentation holds), we can estimate our expected double tag to single tag ratio as follows: From the luminosity, we calculate the number of $e^+e^- \rightarrow c\bar{c}$ events using as inputs the $e^+e^- \rightarrow q\bar{q}$ cross-section (3.3 nb), and taking $\frac{e^+e^- \rightarrow c\bar{c}}{e^+e^- \rightarrow q\bar{q}}=0.4$. Assuming that $f_{correlated}$ is equal to unity for $D|\bar{D}$ events, we can solve Eqn. (4) for $\epsilon_{geometry}$ by comparing the total number of $D^0|\bar{D}^0$ and $D^+|D^-$ double tags we would expect to find (assuming independent fragmentation) with the actual number of $D^0|\bar{D}^0$ and $D^+|D^-$ double tags. This is calculated to be

$$\epsilon_{geometry} = \frac{(2099)(0.4)(3.3)(13.6 \times 10^6)}{(352294/2)^2} \equiv 1.21 \pm 0.04 \text{ (statistical errors only),}$$

using the total luminosity $\mathcal{L}=13.6 \text{ fb}^{-1}$, and the single tag and double tag values for our D^0 and $D^0|\bar{D}^0$ samples, respectively. For the D^+ and $D^+|D^-$ samples, we obtain $\epsilon_{geometry} = 1.21 \pm 0.09$.

Using a value of $\epsilon_{geometry} \equiv 1.21$, a similar calculation can be performed for the expected number of $\Lambda_c^+|\bar{\Lambda}_c^-$ double tags, based on the total number of $c\bar{c}$ events and the single tag yield, giving an expected value of 83.0 ± 2.6 (statistical error only) double tag events. This number is then compared to the measured number of $\Lambda_c^+|\bar{\Lambda}_c^-$ double tags to obtain an estimate of $f_{correlated} = \frac{253 \pm 37}{83.0 \pm 2.6} = 3.04 \pm 0.45$. Despite the roughness of this approach, the observed enhancement is consistent with our calculated production ratios.

IV. STUDY OF THE $\Lambda_c^+|\bar{\Lambda}_c^-$ SIGNAL CHARACTERISTICS

We have compared some of the production characteristics of the observed $\Lambda_c^+|\bar{\Lambda}_c^-$ signal with the $\Lambda_c^+|\bar{D}^0$ and $\Lambda_c^+|D^-$ signals. No obvious difference is found in either the Λ_c^+ momentum spectrum (or $\bar{\Lambda}_c^-$, in the charge conjugate case) or the polar angle distribution of the Λ_c^+ (see Figs. 7 and 8, respectively) for the $\bar{\Lambda}_c^-$ -tagged or the \bar{D} -tagged samples. We also find that the observed $\Lambda_c^+|\bar{\Lambda}_c^-$ cross-section is statistically the same for the data taken on the $\Upsilon(4S)$ resonance as data taken just below the $\Upsilon(4S)$. As expected (Figure 9) if the charmed baryons are following the direction of the original charm/anticharm quarks, the observed opening angle between the Λ_c^+ and $\bar{\Lambda}_c^-$ peaks at 180° . Finally, to investigate the possibility that the $\Lambda_c^+|\bar{\Lambda}_c^-$ signal was associated with the production of a 4-baryon system, we plot the double tag yield in cases where there are well-identified protons found in the same event (Fig. 10). No signal is observed in such a case.

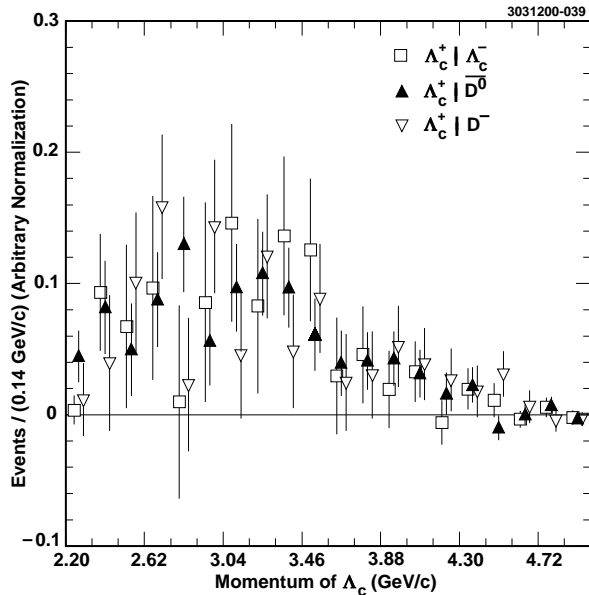


FIG. 7. Λ_c (and charge conjugate) momentum distribution for the three double tag signals $\Lambda_c^+|\bar{\Lambda}_c^-$, $\Lambda_c^+|\bar{D}^0$, and $\Lambda_c^+|D^-$. Squares represent the $\Lambda_c^+|\bar{\Lambda}_c^-$ signal, upright triangles represent the $\Lambda_c^+|\bar{D}^0$ signal, and inverted triangles represent the $\Lambda_c^+|D^-$ signal. These three distributions are qualitatively similar, indicating similar production dynamics. All distributions have been normalized to have unit area.

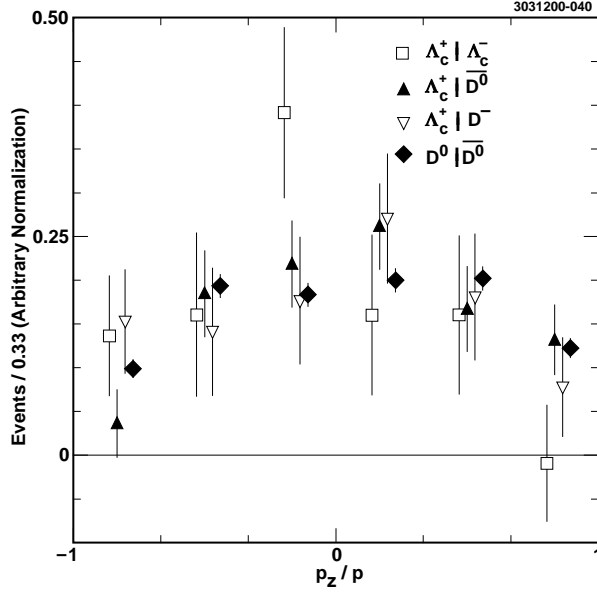


FIG. 8. Polar angle distribution with respect to the e^+e^- beam axis (p_z/p) for the double tag signals $\Lambda_c^+|\bar{\Lambda}_c^-$ (squares), $\Lambda_c^+|\bar{D}^0$ (triangles), $\Lambda_c^+|D^-$ (inverted triangles), and $D^0|\bar{D}^0$ (diamonds). All distributions have been normalized to have unit area.

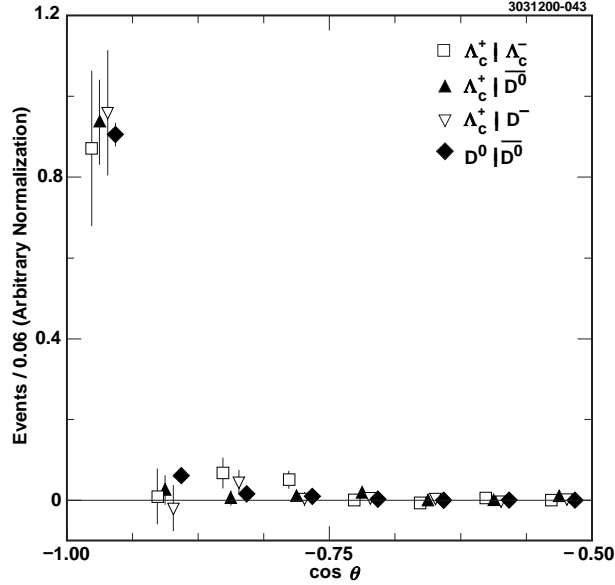


FIG. 9. Production angle between the Λ_c^+ and $\bar{\Lambda}_c^-$ (squares) compared with $\Lambda_c^+|\bar{D}^0$ (upright triangle), $\Lambda_c^+|D^-$ (inverted triangle), and $D^0|\bar{D}^0$ (diamond) event samples. As expected, Λ_c^+ are produced back-to-back with respect to $\bar{\Lambda}_c^-$ tags. All distributions have been normalized to have unit area.

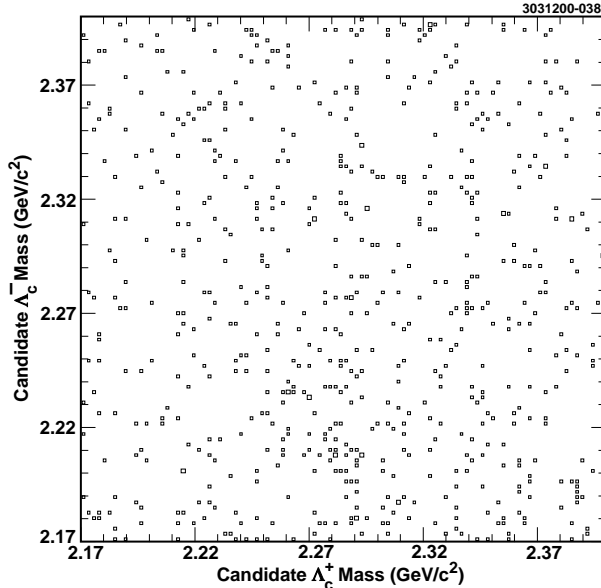


FIG. 10. Double-tag $\Lambda_c^+|\bar{\Lambda}_c^-$ signal in events containing an identified antiproton or proton.

V. $\Sigma_C (\frac{1}{2})^+$ PRODUCTION

We have also investigated the possibility of correlated $\Sigma_c|\bar{\Sigma}_c$ production. Of particular interest here is the possibility of observing an enhanced production rate relative to our observed $\Lambda_c|\bar{\Lambda}_c^-$ correlation. Such an enhancement may be indicative of spin correlations at the first rank in fragmentation. Σ_c 's are reconstructed through their decay mode into Λ_c and a soft pion π_s : $\Sigma_c \rightarrow \Lambda_c\pi_s$. For the highest efficiency and best resolution, only charged pions π_s^\pm are used in reconstructing Σ_c 's. Although statistically limited, a direct search for $\Sigma_c|\bar{\Sigma}_c$ double tags yields 6 events in the signal region (Figure 11); the extrapolated background under the signal is 1.8 ± 0.3 events.

Using the total number of Σ_c single tags observed (3804 ± 185), the total number of Λ_c single tags observed (70199 ± 1604), and the total number of $\Lambda_c|\bar{\Lambda}_c^-$ double tags observed (252.5 ± 37.4), we can estimate the number of expected $\Sigma_c|\bar{\Sigma}_c$ double tags (assuming that the $\Sigma_c|\bar{\Sigma}_c$ correlated production rate is the same as the correlated $\Lambda_c|\bar{\Lambda}_c^-$ production rate) as: $252.5 \times (\frac{3804}{70199})^2 = 0.74 \pm 0.11$. We therefore see a statistically very limited indication of $\Sigma_c|\bar{\Sigma}_c$ correlations, suggesting a spin correlation at the first step of fragmentation. More data are necessary to elucidate this situation.

VI. SYSTEMATICS

We expect most of the systematic uncertainties associated with measurement of both numerator and denominator of the production rates to cancel in calculation of the production ratios. The sensitivity to the definition of “signal” and “sideband” mass regions in the one- and two-dimensional subtraction was determined by calculating the yields as we vary these parameters. We assign a systematic error of 6% due to “signal parameterization uncertainty” based on this study. We have also performed a second (complete) set of fits using two-dimensional Gaussian parameterizations of the signal and two-dimensional polynomial parameterizations of the background. The two techniques

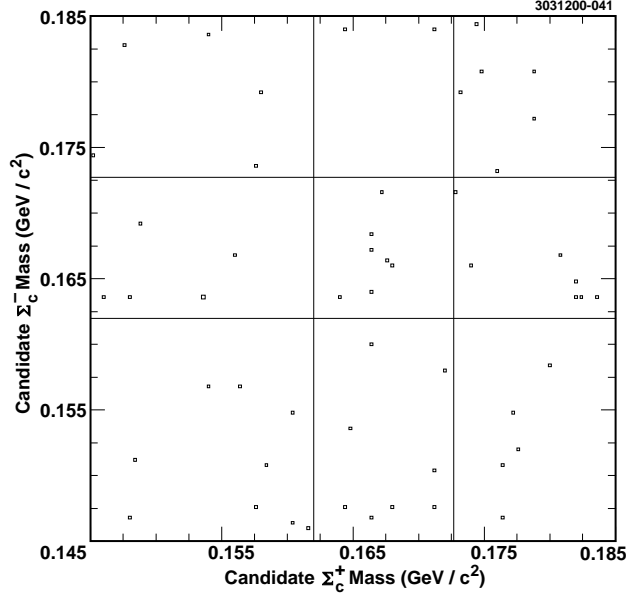


FIG. 11. Double-tag $\Sigma_c|\bar{\Sigma}_c$ mass difference plot. Horizontal and vertical solid lines designate signal bands.

show excellent agreement, and are typically within 5% of each other, for each two-dimensional extraction. When we vary the selection criteria (e.g., particle identification criteria, and minimum momentum requirements) used to define our hadrons (Λ_c , D^0 , and D^+), we observe a maximum 7% variation in the production ratios we calculate. As an example of our investigation of the momentum dependence of the $\Lambda_c^+\bar{\Lambda}_c^-$ production ratio enhancement, Table VII shows the production ratio in the two-dimensional ($p_{\Lambda_c}, p_{\bar{H}_c}$) space.

TABLE VII. Production ratio enhancement tabulated as a function of Λ_c momentum and also the tag momentum in the production rate denominator. For example, the upper left entry (3.02 ± 0.95) represents the production ratio $\frac{\Lambda_c^+|\bar{\Lambda}_c^-}{\Lambda_c} \div \frac{\Lambda_c^+|\bar{D}^0}{D^0}$, for the case where the Λ_c , $\bar{\Lambda}_c^-$, and \bar{D}^0 each have momentum between 2.3 and 3.3 GeV/c. Statistical errors only are shown.

	$2.3 \text{ GeV}/c < p(\Lambda_c) < 3.3 \text{ GeV}/c$	$3.3 < p(\Lambda_c) < 5.0 \text{ GeV}/c$
$2.3 \text{ GeV}/c < p(\bar{\Lambda}_c^-), p(\bar{D}^0) < 3.3 \text{ GeV}/c$	3.02 ± 0.95	4.04 ± 1.93
$3.3 \text{ GeV}/c < p(\bar{\Lambda}_c^-), p(\bar{D}^0) < 5.0 \text{ GeV}/c$	2.60 ± 1.23	3.79 ± 1.51
$2.3 \text{ GeV}/c < p(\bar{\Lambda}_c^-), p(D^-) < 3.3 \text{ GeV}/c$	3.30 ± 1.33	3.42 ± 1.99
$3.3 \text{ GeV}/c < p(\bar{\Lambda}_c^-), p(D^-) < 5.0 \text{ GeV}/c$	3.39 ± 1.76	3.50 ± 1.47

The systematic errors are added, mode-by-mode, to determine the overall systematic error for each calculated production ratio (Table IV).

VII. SUMMARY

The measured values of the production ratios imply that a Λ_c is roughly three times more likely to be produced opposite a $\bar{\Lambda}_c$ than opposite either a \bar{D}^0 or a D^- . These results indicate strong evidence in support of correlated production of the Λ_c . Assuming that 6% of charm quark fragmentation at $\sqrt{s} \sim 10$ GeV results in a charmed baryon, our result implies that approximately 20% of all Λ_c 's are produced in association with a $\bar{\Lambda}_c^-$ in the opposite hemisphere. The effect is not produced by the Jetset simulation but does not contradict the Lund String Model. In fact if the primary $c\bar{c}$ were broken at very small proper time by diquark-antidiquark tunneling from the vacuum, producing a (possibly excited) charm baryon system and anti-charm antibaryon system, a correlation of the type observed here would be generated.

VIII. ACKNOWLEDGMENTS

We gratefully acknowledge the effort of the CESR staff in providing us with excellent luminosity and running conditions. M. Selen thanks the PFF program of the NSF and the Research Corporation, A.H. Mahmood thanks the Texas Advanced Research Program, F. Blanc thanks the Swiss National Science Foundation, and E. von Toerne thanks the Alexander von Humboldt Stiftung for support. This work was supported by the National Science Foundation, the U.S. Department of Energy, and the Natural Sciences and Engineering Research Council of Canada.

REFERENCES

- [1] T. Gottschalk, Nucl. Phys. **B214**, 201 (1983); G. Marchesini and B.R. Webber, Nucl. Phys. **B238**, 1 (1984); B.R. Webber, Nucl. Phys. **B238**, 492 (1984); T. Gottschalk and D. Morris, Nucl. Phys. **B288**, 729 (1987).
- [2] B. Andersson, G. Gustafson, G. Ingelman and T. Sjostrand, Phys. Rep. **91** (1983) 31; B. Andersson, “The Lund Model”, Cambridge University Press, 1998.
- [3] X. Artru and G. Menessier, Nucl. Phys. **70** 93, (1974); X. Artru, Phys. Rep. **97**, 1 (1983).
- [4] V.G. Kartvelishvili, A.K. Likhoded and S.R. Slobospitskii, Sov. Jour. Nucl. Phys. **33**, 434 (1981).
- [5] R. Vogt and S.J. Brodsky, Nucl. Phys. **B478**, 311 (1996).
- [6] J.C. Anjos, G. Herrera, J. Magnin and F.R.A. Simão, Phy. Rev. **D56**, 394 (1997).
- [7] PYTHIA 5.7 and JETSET 7.4 Physics Manual, CERN-TH-7112/93(1993); H.U. Bengtsson and T. Sjostrand, Comp. Phys. Comm. **46**, 43 (1987); T. Sjostrand, CERN-TH.7112/93 (1993).
- [8] The OPAL Collaboration, G. Abbiendi et al., Eur. Phys. J. **C10**, 547 (1999)
- [9] The CLEO Collaboration, Y. Kubota *et al.* , Nucl. Instrum. Methods Phys. Res. A **320**, 66 (1992).
- [10] T. S. Hill *et al.*, Nucl. Inst. Meth. Phys. Res., Sec. A**418**, 32 (1998).
- [11] X. Artru and G. Menessier, Nucl. Phys. **70** (1974) 93; B. Andersson, G. Gustafson, G. Ingelman and T. Sjostrand, Phys. Rep. **97** (1983) 33; X. Artru Phys. Rep. **97**, 147 (1983) for example.